MATHEMATICS AND COMPUTATIONAL SCIENCES

Vol 3(3), 2022, pp: 11-28
DOI:10.30511/mcs.2022.544481.1057
ISSN:2717-2708
http://mcs.qut.ac.ir/

Qom University of Technology

Second-Order Slip Effect on the Flow of MHD Chemically Reacting Fluid Through an Inclined Micro-Annular Channel

Timothy. L. Oyekunle[1], Mojeed. T. Akolade[2]*, Samson A. Agunbiade[3], Hafizat O. Momoh[4]

Abstract: This study explores the second-order slip effect on the flow of MHD chemically reacting fluid through an inclined micro-annular channel. As knowledge in flow and heat transfer is showcased in macro/micro-channel areas, consistent advancement is essential to familiar with fundamental phenomena associated. The free convection study encompasses the temperature-dependent viscosity and uniform magnetic field effect. The dimensionless equations governing the flow are modeled and solved semi-analytically via Akbari-Ganji's Method (AGM). The velocity, energy, concentration and physical characteristics of the flow results are obtained and discussed with the aid of tables and graphs. It is found that a higher value of the slip parameter diminishes the velocity distribution at the annular gap and surfaces, while, the temperature-dependent exponential variability model enhances the fluid velocity.

Keywords: AGM, Micro-Annular channel; Slip flow; MHD; Fully developed flow; Continuum regime.
2020 Mathematics Subject Classification: 76M55; 65L80; 65L06; 34B15; 34B60.
Receive: 8 Desember 2021, **Accepted:** 16 September 2022

1 Introduction

In recent times, there has been renewed attention in the investigations of the fully developed flow of magnetohydrodynamics (MHD), a free convective process through annular micro-channel with slip and jump conditions. Physical processes in which buoyancy forces emanate from both thermal and spices diffusion play a significant role in convective mass transfer and heat analysis. This application can be found in electronics power generation, MHD pumps, and chemical industries (Rajasekhar [32]). Also, the cooling of store grain, geothermal system usage, oil extraction, groundwater pollution, storage of nuclear wastes, and thermal insulation are significant applications of heat and mass transfer (Yusuf and Jha [39]). Considering the adherence of the fluid

[1] Department of Mathematics University of Ilorin, Ilorin, Nigeria, Email: tloyekunle95@gmail.com
[2]*Corresponding author: Department of Mathematics University of Ilorin, Ilorin, Nigeria, Email: akolademojeed@yahoo.com
[3] Department of Mathematics Babcock University Ilishan-Remo, Ogun State, Nigeria, Email: agunbiade1971@gmail.com
[4] Department of Mathematics and Statistics Federal Polytechnic Nasarawa State, Nigeria, Email: ozichuhafizat@gmail.com

particles and the solid boundary, the absence of the slip model is found faulty in many applications such as micro-channel flow, and the model of thin fluid among others (Liu and Guo [24]). Therefore, it is imperative to investigate the flow of the second-order slip effect in MHD chemically reacting fluid through an inclined micro-annular channel considering its application occurrence both in industries and nature.

In view of these applications, motivated researchers such as Ameel et al. [6] gave the effects of heat flux and slip flow on forced convection in a circular tube. They highlighted that the fully developed heat transfer coefficient reduces with the Knudsen number at the wall. In the modeling of oscillatory hydro-magnetic flow, Rajasekhar et al. [32] examined a free convective flow and coupled stress fluid through an inclined rotating channel. While investigations of vertically double-diffusive natural convective flow through the annular porous medium is examined by Jha et al. [22], they noticed that the inclusion of thermal diffusion slows down the flow rate analysis. Jha et al. [20] examined the flow through a vertical annular microchannel subjected to natural convective and MHD effects. They realized that a rise in curvature radius speeds up the volume flow rate. The study of slip flow between parallel micro-channel plates was analyzed by Saghafian et al. [34], they reported that the Nusselt number decreases with an increase in refraction and proved that the perturbation method with a higher magnitude of Knudsen number predicts the temperature and velocity field accurately. Heat absorption in vertically concentric annulus channel was presented by Yusuf [38], the study gave an exact solution of the MHD effect in natural convection. He discovered that the size of maximum fluid velocity is greater in the isothermal heating case compared to that of the constant heat flux case when the radius of the outer cylinder is less or equal to the inner cylinder. On the other hand, Reddy et al. [33] analyzed the fluid flow over a rotating disk coupled with chemically reacting Ag-and Cu-water traveling nanofluid via a porous medium. The investigation shows that the temperature is elevated with a rise in nanoparticle volume fraction parameters.

Recently, Idowu et al. [18] analyzed the nonlinear convective flow through an Annular channel, Akolade et al. [5] investigated MHD flow through a squeezed channel, and Idowu et al. [19] presented the numerical solutions to dissipative Casson nanofluid through the annular medium, Oyekunle and Agunbiade [31] combined the effect of viscosity and thermal radiation in MHD fluid flow examination through an irregular channel. Atashafrooz and Asadi [7] gave the irreversibility analysis of buoyancy force through an inclined Duct. While Okedayo and Salawu [29] investigated the MHD flow of Newtonian fluid with variable viscosity and thermal conductivity influences. The flow of reactive species in an oscillatory annular channel is discussed by Debnath et al. [10] where the radii ratio is seen to give a mixed behavior of the dispersion coefficient. Oni and Jha [30] experimented the heat absorption/generation with time-periodic boundary conditions on free convection flow through a vertical annulus. They observed that, at the surface of the cylinders, the heat absorption/generation parameter decreases/increases periodic temperature distribution and velocity profile respectively.

All things been equal, the study of slip and jump conditions has not been left out due to its physical phenomenon. Therein, the modeling of dissipative fluid through a micro-tube encompassing the viscous heating within the medium and jump condition at the wall is investigated by Tunc and Bayazitoglu [36]. Makinde and Osalusi [25] presented the wall velocity slip and MHD effects through a uniform channel width. The flow through a long isoflux and isothermal force convection heated/cooled planner micro-channel in the presence of second-order slip and jump condition is presented by Huel [14]. He observed that the thermal creep becomes more significant and a higher magnitude of second-order slip increases the flow velocity and decreases the heat flux accordingly, while Hui and Chien-Hung [15] show that a rise in Knudsen number pronounces the second-order slip effect in an isothermal condition.

Zhu et al. [40] investigated the influences of second-order slip and jump conditions on third-grade nanofluids over a coaxial tube. They reported that the thermophoresis movement and Brownian motion resulted

in a rise in temperature distribution. Adesanya [1] presented a slip flow and jump condition through a porous vertical medium of heat-generating fluid. He realized that a rise in slip and jump conditions speeds up the rate of flow velocity and temperature accordingly. Khan et al. [23] enumerated the combined effects of slip and variable viscosity in an inclined asymmetric channel. In an analytical study of asymmetric mini/micro-channel filled with microfoam, Xu et al. [37] considered the thermal and velocity slip among other quantities, hence, the solution procedure was seen to predict the flow distributions accurately while a decrease in slip flow region is pronounced to a higher magnitude of Knudsen number. Recently, two different boundary conditions were imposed on the flow of non-linear radiative vertical channels containing MHD nanofluid by Ibanez et al. [16]. Avramenko et al. [8] presented the analytical solution of second-order slip flow in a microconfusor. They noticed that all fluid characteristics were affected while varying the second-order slip parameter except the heat transfer coefficient.

Solving non-linear systems of ODEs and PDEs becomes more imperative due to their real-life modeling instances, hence, to overcome these challenges, several semi-analytical and numerical methods over the years have been developed among which: Differential Transformation Method (DTM), Adomian Decomposition Method (ADM), Homotopy Analysis Method (HAM), Variational Iteration Method (VIM), Lyapunov's small parameter method among others had proven their effectiveness, convergent, and efficiency in problem-solving. However, to solve non-linear differential equations, Akbari et al. [3] proposed an innovative algebraic approach called Akbari-Ganji's Method (AGM). While Ahmadi et al. [2] presented a detailed analysis of this method for solving integro-differential, non-linear, vibrational, and non-vibrational equations. Chakraverty et al. [9] demonstrated several numerical examples applying this recent semi-analytical approach to initial value problems. Investigations on heat transfer analysis using AGM were studied in (Mirgolbabaee et al. [26], [27], [28], Sheikholeslami and Ganji [35]). AGM was as well employed by Ghadikolaei et al. [13] to investigate the squeezing stretching channel flow of an unsteady MHD Eyring-Powell fluid. Recently, Dharmalingam and Veeramuni [11] employed this method to determine the substrate concentration in an electroactive polymer film. On this note, AGM is found satisfactorily good for solving channel problems.

In view of this literature, to our best knowledge, no attention has been paid to the second-order slip effect on MHD chemically reacting fluid flow through an inclined micro-annular channel. Therefore, this has drawn the attention of the authors to carry out the present study. The impact of some embedded parameters such as the Buoyancy ratio, radii ratio, inclined angle, and slip parameter among others on the flow characteristics was discussed vividly. The dimensionless equations governing the fluid flow were solved using AGM with MAPLE 18 symbolic package.

2 Mathematical model formulation

An electrically conducting, incompressible, two-dimensional, steady, free convective fully developed flow of viscous fluid through an infinite micro-annular channel inclined at an angle α is considered. The annular region is made up of the inner and outer cylinders of radius r_1 and r_2 respectively. The $y-$axis is taken parallel to the flow direction while $\omega-$ axis is perpendicular to $y-$axis as shown in Fig. 1.

The inner and outer cylinders are at constant temperature T_1 and T_2, concentration ϕ_1 and ϕ_2 respectively. All fluid properties were presumed constant except the viscosity (assumed temperature-dependent) and the

density in the buoyancy force represented by $\rho_0(1-\beta_m(\bar{T}-T_0)-\beta_n(\bar{\phi}-\phi_0))$. The magnetic field induced is considered small and thus neglected. Hence, the equations governing the fluid flow based on the usual Boussinesq approximation are as follows (See Idowu et al [17], [18], [19]).

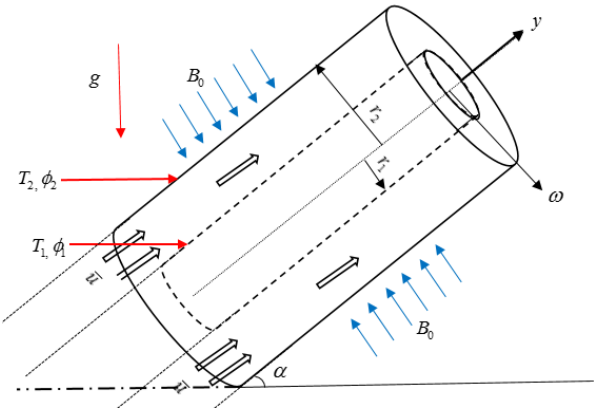

Fig. 1. The physical coordinate system of the model.

$$\frac{1}{\omega}\frac{d}{d\omega}\left[\omega\mu(T)\frac{d\bar{u}}{d\omega}\right]-\sigma B_0^2\bar{u}+g\rho_0\cos\alpha\left[\beta_m(\bar{T}-T_0)+\beta_n(\bar{\phi}-\phi_0)\right]=0, \tag{2.1}$$

$$\frac{k_0}{\rho c_p\omega}\frac{d}{d\omega}\left[\omega\frac{d\bar{T}}{d\omega}\right]+\frac{Q_0}{\rho c_p}(\bar{T}-T_0)=0, \tag{2.2}$$

$$\frac{D_B}{\omega}\frac{d}{d\omega}\left[\omega\frac{d\bar{\phi}}{d\omega}\right]-Kr(\bar{\phi}-\phi_0)=0, \tag{2.3}$$

The appropriate boundary conditions encompassing the effects of first and second-order slips, temperature jump, and constant concentration are; (Huel [14], Jha, et al. [22], and [20])

$$\begin{aligned}&\bar{u}(\omega)=\beta_v\lambda_d\frac{d\bar{u}(\omega)}{d\omega}+\gamma\lambda_d^2\frac{d^2\bar{u}(\omega)}{d\omega^2},\ \bar{T}(\omega)-T_1=\beta_t\lambda_d\frac{d\bar{T}(\omega)}{d\omega},\bar{\phi}(\omega)=\phi_1\text{ at }\omega=r_1,\\&\bar{u}(\omega)=-\beta_v\lambda_d\frac{d\bar{u}(\omega)}{d\omega}+\gamma\lambda_d^2\frac{d^2\bar{u}(\omega)}{d\omega^2},\ \bar{T}(\omega)-T_2=-\beta_t\lambda_d\frac{d\bar{T}(\omega)}{d\omega},\bar{\phi}(\omega)=\phi_2\text{ at }\omega=r_2,\end{aligned} \tag{2.4}$$

The temperature-dependent viscosity variation is presented accordingly (Akolade et al. [4], Jha et al. [21], and Gbadeyan et al. [12]),

$$\mu(T)=\mu_0\exp[-b(\bar{T}-T_0)], \tag{2.5}$$

μ_0 represent the viscosity at T_0, and strength dependency between $\bar{T}$ and μ depends on the coefficient b.

Introducing the following dimensionless variables, along with equation (2.5), into (2.1) – (2.4)

$$Z = \frac{\omega - r_1}{\eta}, \eta = r_2 - r_1, \; u = \frac{\bar{u}}{U_m}, \gamma = \frac{9}{4\pi}\frac{\gamma_r - 1}{\gamma_r}\Pr, \; \theta = \frac{\bar{T} - T_0}{T_1 - T_0}, \; \phi = \frac{\bar{\phi} - \phi_0}{\phi_1 - \phi_0}, \; \xi = \frac{r_1}{r_2},$$

$$\lambda_d = \frac{\sqrt{\pi \bar{R} T / 2\mu}}{\rho_0}, \; \chi = 1 - \xi, \; U_m = \frac{\rho_0 g \beta_m (T_1 - T_0)}{\mu_0}\eta^2$$

Thus, the governing equations (2.1) - (2.4) are reduced to;

$$\frac{1}{\chi Z + \xi}\frac{d}{dZ}\left[(\chi Z + \xi)\exp(-B\theta)\frac{du}{dZ}\right] - M^2 u + \cos(\alpha)\left[\theta + Br\,\phi\right] = 0, \tag{2.6}$$

$$\frac{1}{\chi Z + \xi}\frac{d}{dZ}\left[(\chi Z + \xi)\frac{d\theta}{dZ}\right] + H_0\,\theta = 0, \tag{2.7}$$

$$\frac{1}{\chi Z + \xi}\frac{d}{dZ}\left[(\chi Z + \xi)\frac{d\phi}{dZ}\right] - Sc\,\lambda\,\phi = 0, \tag{2.8}$$

Subject to the boundary conditions

$$\begin{aligned} u(Z) &= \beta_v Kn\frac{du(Z)}{dZ} + \gamma Kn^2\frac{d^2u(Z)}{dZ^2}, \; \theta(Z) = 1 + \beta_v KnP\frac{d\theta(Z)}{dZ}, \; \phi(Z) = 1 \text{ at } Z = 0, \\ u(Z) &= -\beta_v Kn\frac{du(Z)}{dZ} + \gamma Kn^2\frac{d^2u(Z)}{dZ^2}, \; \theta(Z) = -\beta_v KnP\frac{d\theta(Z)}{dZ}, \; \phi(Z) = Rc \text{ at } Z = 1. \end{aligned} \tag{2.9}$$

Where,

$$B = b(T_1 - T_0), \; \beta_t = \frac{2 - \sigma_t}{\sigma_t}\frac{2\epsilon}{\epsilon + 1}\frac{1}{\Pr}, \; \beta_v = \frac{2 - \sigma_m}{\sigma_m}, \; M = B_0\eta\sqrt{\frac{\sigma}{\rho_0 \nu}}, \; Br = \frac{\beta_n(\phi_1 - \phi_0)}{\beta_m(T_1 - T_0)},$$

$$Rc = \frac{\phi_2 - \phi_1}{\phi_1 - \phi_0}, \; H_0 = \frac{Q_0}{\kappa}\eta^2, \; \lambda = \frac{Kr\,(1 - \xi)^2}{\nu}, \; Sc = \frac{\nu}{D_B}, \; P = \frac{\beta_t}{\beta_v}, \; Kn = \frac{\lambda_d}{\eta}, \; \Pr = \frac{c_p \nu_0}{\kappa}.$$

The characteristics of the convective flow, Sherwood number, Nusselt number, volumetric flow rate, and skin friction were analyzed.

The volumetric flow rate;

$$Q = 2\pi\int_0^1 Z u(Z) dZ. \tag{2.10}$$

The Sherwood number (Sh), Nusselt number (Nu), and Skin-friction (τ^*) at the annulus surfaces are obtained as follows:

$$\tau^*_{0,1} = \exp(-B\,\theta)\frac{du}{dZ}\Big|_{Z=0,1}, \; Nu_{0,1} = \frac{d\theta}{dZ}\Big|_{Z=0,1}, \; Sh_{0,1} = \frac{d\phi}{dZ}\Big|_{Z=0,1} \tag{2.11}$$

3 Semi-Analytical Solution

Subject to the boundary conditions (2.9), the governing problems (2.6) - (2.8) were solved semi-analytically using AGM fully documented in (Akbari et al. [3], Ahmadi et al. [2], Chakraverty et al. [9], Mirgolbabaee et al. [26], [27], [28], Sheikholeslami and Ganji [35] Ghadikolaei et al. [13], Dharmalingam and Veeramuni [11]) of which found satisfactorily good for solving channel problems.

Representing the left-hand side of equations (2.6) - (2.8) in the following order:

$$\mathrm{U(Z)} := \frac{1}{\chi \mathrm{Z}+\xi}\frac{\mathrm{d}}{\mathrm{dZ}}\left[\left(\chi \mathrm{Z}+\xi\right)\exp(-\mathrm{B}\theta)\frac{\mathrm{du}}{\mathrm{dZ}}\right]-\mathrm{M}^2\mathrm{u}+\cos(\alpha)\left[\theta+\mathrm{Br}\,\phi\right], \tag{3.1}$$

$$\Theta(\mathrm{Z}) := \frac{1}{\chi \mathrm{Z}+\xi}\frac{\mathrm{d}}{\mathrm{dZ}}\left[(\chi \mathrm{Z}+\xi)\frac{\mathrm{d}\theta}{\mathrm{dZ}}\right]+\mathrm{H}_0\,\theta, \tag{3.2}$$

$$\Phi(\mathrm{Z}) := \frac{1}{\chi \mathrm{Z}+\xi}\frac{\mathrm{d}}{\mathrm{dZ}}\left[(\chi \mathrm{Z}+\xi)\frac{\mathrm{d}\phi}{\mathrm{dZ}}\right]-\mathrm{Sc}\,\lambda\,\phi, \tag{3.3}$$

Thus, utilizing the basic idea of AGM, the assumed trial solutions polynomials of degree with constant coefficients are given by:

$$\begin{aligned}
\mathrm{u(Z)} &= \sum_{\mathrm{i}=0}^{\mathrm{N}}\mathrm{a_i Z^i} = \mathrm{a_0}+\mathrm{a_1 Z}+\mathrm{a_2 Z^2}+\mathrm{a_3 Z^3}\ldots,\\
\theta(\mathrm{Z}) &= \sum_{\mathrm{i}=0}^{\mathrm{N}}\mathrm{b_i Z^i} = \mathrm{b_0}+\mathrm{b_1 Z}+\mathrm{b_2 Z^2}+\mathrm{b_3 Z^3}\ldots,\\
\phi(\mathrm{Z}) &= \sum_{\mathrm{i}=0}^{\mathrm{N}}\mathrm{c_i Z^i} = \mathrm{c_0}+\mathrm{c_1 Z}+\mathrm{c_2 Z^2}+\mathrm{c_3 Z^3}\ldots,
\end{aligned} \tag{3.4}$$

Illustrating for N = 9, equation (3.4) is computed to obtain the constants coefficients a_N, b_N and c_N accordingly, by employing the boundary conditions we have (Mirgolbabaee et al. [28]).

(i) Applying equation (3.4) on (2.9) generates the following systems accordingly:

$$
\begin{aligned}
&u(0) \Rightarrow a_0 = \beta_v \mathrm{Kn}\chi a_1 + \gamma \mathrm{Kn}^2\chi^2 2a_2,\\
&u(1) \Rightarrow a_0 + a_1 + a_2 + a_3 + a_4 + a_5 + a_6 + a_7 + a_8 + a_9 = -\beta_v \mathrm{Kn}\chi(a_1 + 2a_2 +\\
&\qquad 3a_3 + 4a_4 + 5a_5 + 6a_6 + 7a_7 + 8a_8 + 9a_9) + \gamma \mathrm{Kn}^2\chi^2(2a_2 + 6a_3 +\\
&\qquad 12a_4 + 20a_5 + 30a_6 + 42a_7 + 56a_8 + 72a_9),\\
&\theta(0) \Rightarrow b_0 = 1 + \beta_v \chi \mathrm{Kn}\,\mathrm{P}b_1\\
&\theta(1) \Rightarrow b_0 + b_1 + b_2 + b_3 + b_4 + b_5 + b_6 + b_7 + b_8 + {}_9 =\\
&\qquad -\beta_v \mathrm{Kn}\chi \mathrm{P}(b_1 + 2b_2 + 3b_3 + 4b_4 + 5b_5 + 6b_6 + 7b_7 + 8b_8 + 9b_9),\\
&\phi(0) \Rightarrow c_0 = 1,\\
&\phi(1) \Rightarrow c_0 + c_1 + c_2 + c_3 + c_4 + c_5 + c_6 + c_7 + c_8 + c_9 = \mathrm{Rc}.
\end{aligned}
\tag{3.5}
$$

(ii) in equation (3.5) we have 6 equations with 36 unknown coefficients. To generate additional 30 equations, we employed the AGM approach presented in equation (3.6) on main equations (3.1) - (3.3),

$$
\begin{aligned}
&\mathrm{U}(u(Z)) \Rightarrow \mathrm{U}(u(0)) = 0,\ \mathrm{U}'(u(0)) = 0,\ldots\\
&\mathrm{U}(u(Z)) \Rightarrow \mathrm{U}(u(1)) = 0,\ \mathrm{U}'(u(1)) = 0,\ldots\\
&\Theta(\theta(Z)) \Rightarrow \Theta(\theta(0)) = 0,\ \Theta'(\theta(0)) = 0,\ldots\\
&\Theta(\theta(Z)) \Rightarrow \Theta(\theta(1)) = 0,\ \Theta'(\theta(1)) = 0,\ldots\\
&\Phi(\phi(Z)) \Rightarrow \Phi(\phi(0)) = 0,\ \Phi'(\phi(0)) = 0,\ldots\\
&\Phi(\phi(Z)) \Rightarrow \Phi(\phi(1)) = 0,\ \Phi'(\phi(1)) = 0,\ldots
\end{aligned}
\tag{3.6}
$$

Thirty (30) additional equations were generated from the procedure (ii), in addition to the six (6) presented in procedure (i), summing up to thirty-six (36) equations. These equations were solved simultaneously to obtain the required constants coefficients a_N, b_N and c_N accordingly, hence, substituted back into the assumed trial solutions in equation (3.4), to obtain the approximate solutions for $u(Z)$, $\theta(Z)$ and $\phi(Z)$ accordingly.

4 Results and Discussion

The goal of this study is to examine the second-order slip effect on the flow of chemically reacting MHD fluid through an inclined micro-annular channel, by employing AGM, a semi-analytical approach. To get a clear understanding of the physical problem, the flow distribution together with some flow characteristics such as Skin friction, Nusselt number, and Sherwood number are analyzed. Following Jha et al. [22] and Jha et al. [21], we took $\mathrm{Pr} = 0.71$, $\beta_v = 1$, $\mathrm{M} = 2$, $\mathrm{Br} = 1.0$, $\mathrm{H}_0 = 0.1$, $\gamma = 0.5$, $\mathrm{Sc} = 0.7$, $\lambda = 0.1$, $\mathrm{P} = 1.64$, $\alpha = \pi/3$, $\mathrm{Rc} = 0.2$, $\mathrm{B} = 0.5$, $\xi = 0.5$, $\mathrm{Kn} = 0.05$. which are kept constant throughout the study unless otherwise stated in the respective tables and figures. The results are presented both in graphical and tabular form, thus, the conclusions were drawn from the flow distributions and other interesting physical quantities.

A comparison of the present result with the previous work of Jha et al. [20] where an exact approach was utilized in solving the formulated flow problem is presented in Table 1, this was carried out by setting the embedded parameters to zero, thus, an excellent agreement is obtained.

Table 1 Comparison of the velocity (u) and Temperature (θ), by taken, $\xi = 0.8$, $M = 0.5$, $Pr = 0.71$, $P = 1.64$, $\alpha = B = Br = H_0 = \gamma = 0$,

		Velocity profile		Temperature profile	
βKn	Z	Jha et al. [20]	Present study	Jha et al. [20]	Present study
0.00	0.2	0.0460	0.045975	0.7814	0.781351
	0.5	0.0576	0.057580	0.4722	0.472165
	0.7	0.0409	0.040942	0.2773	0.277289
	0.9	0.0145	0.014528	0.0905	0.090537
0.01	0.2	0.0484	0.048440	0.7706	0.770565
	0.5	0.0597	0.059712	0.4713	0.471277
	0.7	0.0430	0.042984	0.2826	0.282640
	0.9	0.0136	0.016294	0.1019	0.101866
0.1	0.2	0.0690	0.069037	0.6976	0.697619
	0.5	0.0786	0.078550	0.4653	0.465275
	0.7	0.0616	0.061591	0.3188	0.318833
	0.9	0.0334	0.033442	0.1785	0.178494

Figures 2 and 3 highlight the convergence analysis of the AGM in the present study. An increase in steps (N) of the assumed trial functions results in a more accurate solution as seen in the respective figures, validating the method used. Figure 4 presents the comparison between the numerical results (R-K 4th order) and AGM results for different values of the radii ratio parameter (ξ) on the velocity profile. It is evident that both methods preserve enough accuracy and efficiency in solving coupled nonlinear differential equations. Meanwhile, it is realized that a rise in ξ enhanced the velocity significantly in the annular gap.

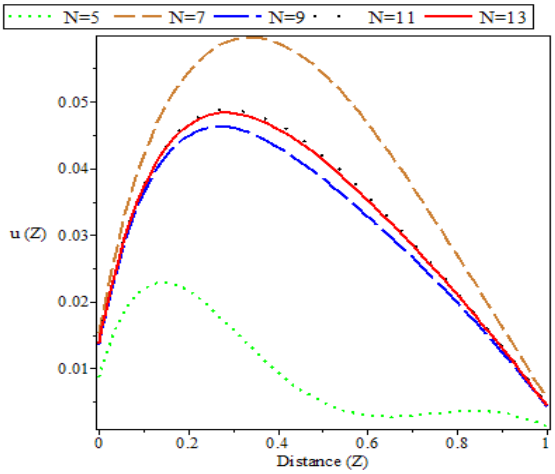

Fig. 2. Increase in steps of the assumed trial functions on u(z)

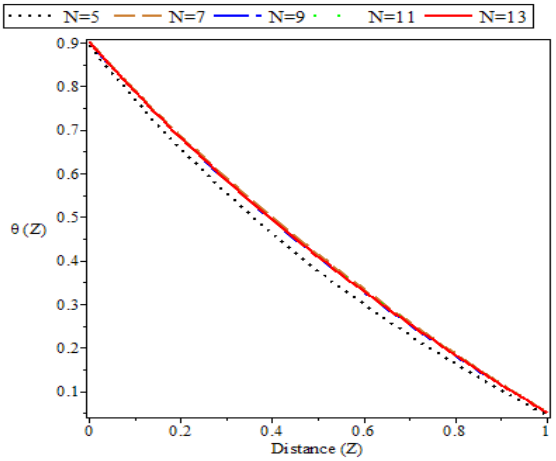

Fig. 3: Increase in steps of the assumed trial functions on $\theta(z)$

Several second-order slip models (Hsia and Domoto, Deissler, Maxwell-Burnett, Kamiadakis) proposed in the literature were presented in Fig. 5, it is seen that a higher second-order slip model reduces the flow velocity both at the annular gap and surfaces. On this note, it is worth mentioning that the slip parameter contributes significantly to the flow distributions as perceived.

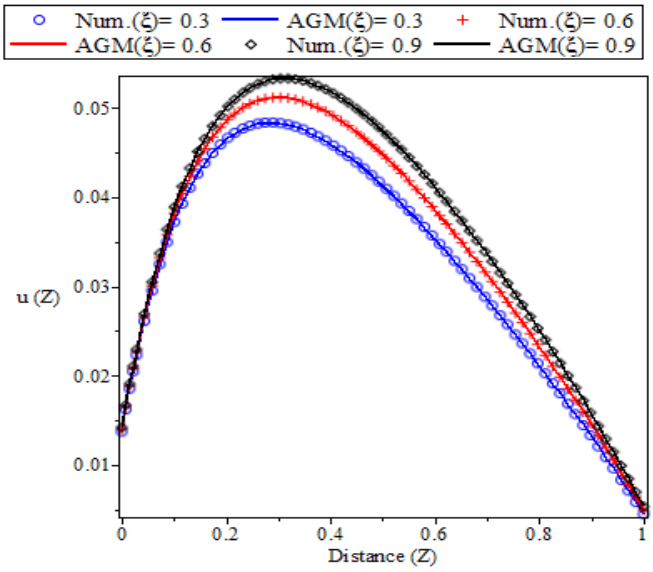

Fig. 4. Comparison between R-K 4th order and AGM results for different values of Radii ratio.

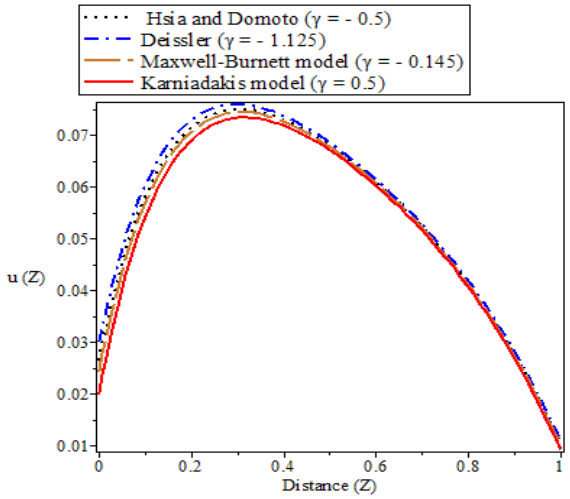

Fig. 5. Effects of Second-order Slip models on u(z).

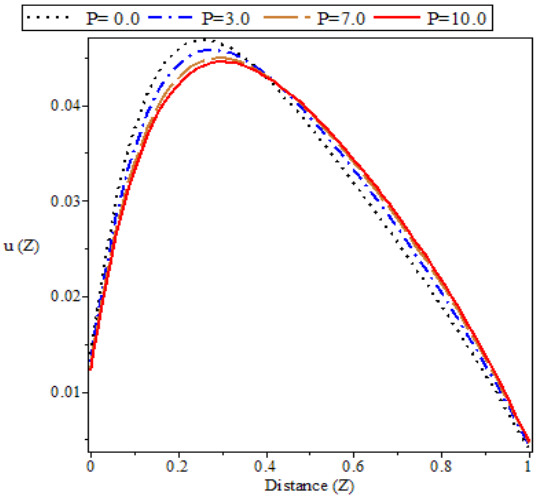

Fig. 6. Effect of Fluid wall interaction on u(z).

Figures 6 and 7 depict the variation of fluid wall interaction on velocity and temperature profile respectively. A rise in P pronounced a decrease in fluid velocity and temperature respectively. While a decrease in slip velocity and temperature near the inner surface of the outer cylinder is observed, the outer surface of the inner cylinder gave an opposing behavior.

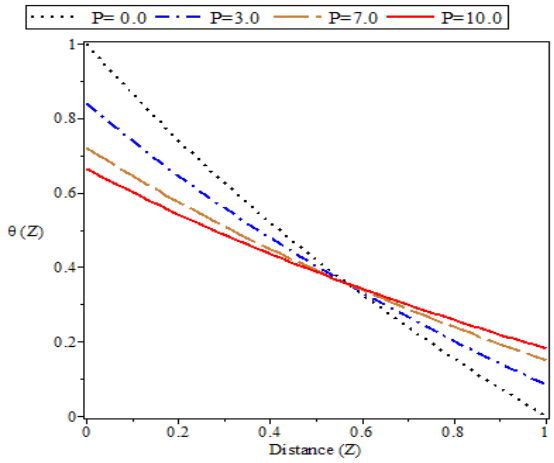

Fig. 7. Effect of Fluid wall interaction on $\theta(z)$.

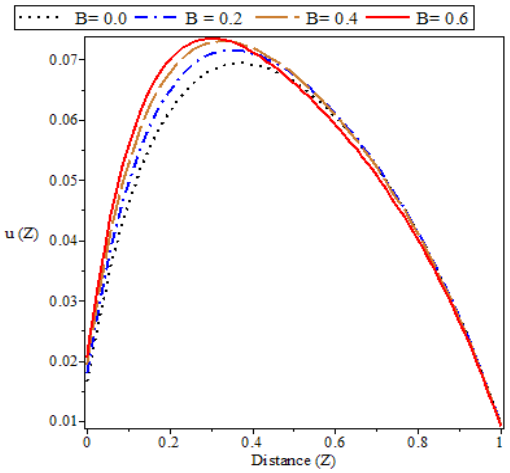

Fig. 8. Variation of variable viscosity on u(z).

The variable viscosity (B) is varied on the velocity profile as shown in Fig. 8. A rise in B appreciates both the fluid velocity and slip velocity at the outer surface of the inner cylinder as a result of an exponential variability model that produces higher velocity. Figures 9 and 10 present the variations of magnetic field parameter (M) and inclined angle (α) on velocity distributions respectively. Both figures gave a declining behavior of velocity

distribution to a higher magnitude of M and α respectively. Physically, the magnetic field exhibits a resistance force known as Lorentz force which is capable of resisting the fluid velocity when the magnetic field is been strengthened, and due to forces acting upon the fluid particles, α reduces the flow field. The presence of slip gives room for the fluid to become more viscous, thus resulting in retardation in fluid velocity and reducing the momentum distributions.

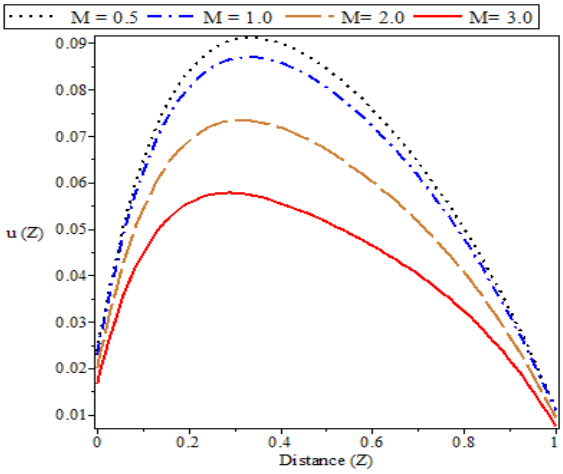

Figure 9: Influence of Magnetic field on the velocity profile.

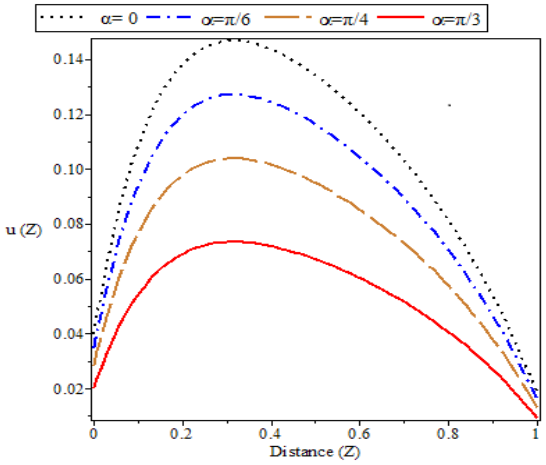

Fig. 10. Influence of Inclined angle on the velocity profile.

Figures 11 and 12 reveal the variation of buoyancy ratio (Br) and wall concentration ratio (Rc) on velocity distribution respectively. With the presence of slip, it is noticed that Br and Rc speed up the velocity profiles at the annular gap and surfaces.

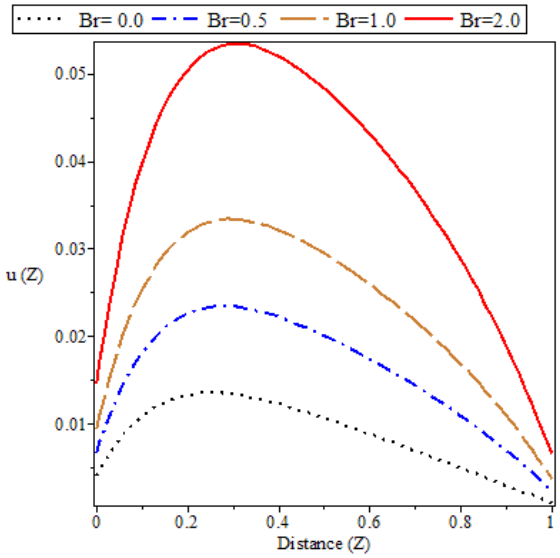

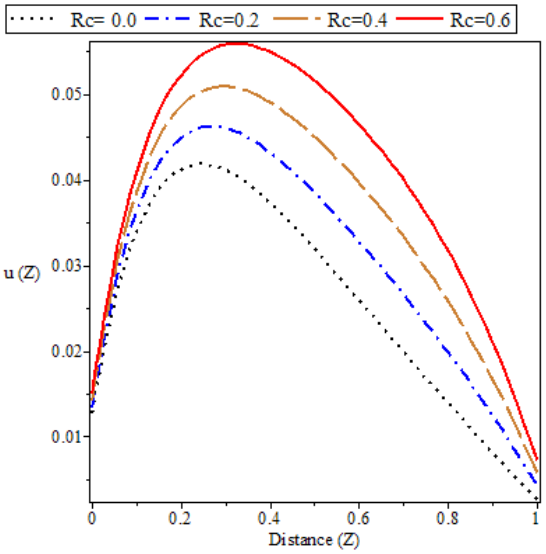

Fig. 11. Variation of Buoyancy ratio on u(z)

Fig. 12. Variation of Wall concentration ratio on u(z)

For $Br = 0$, Fig. 11 shows the least velocity profile, as a result of dominance in solute buoyancy forces in the flow distribution, thus, $Br > 0$, the thermal and solute buoyancy forces tend to act in the same direction, and the flow thus assisted.

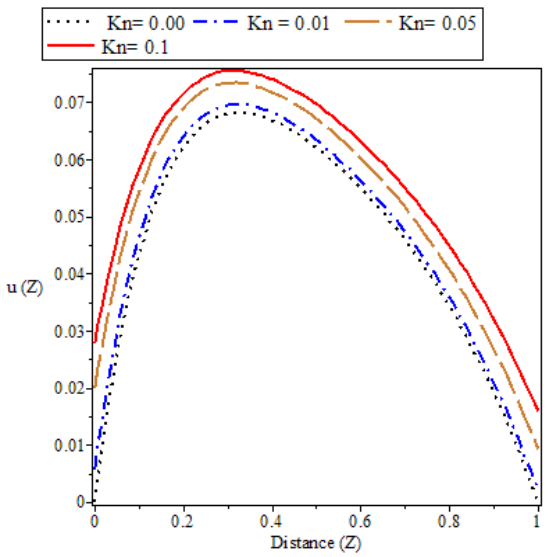

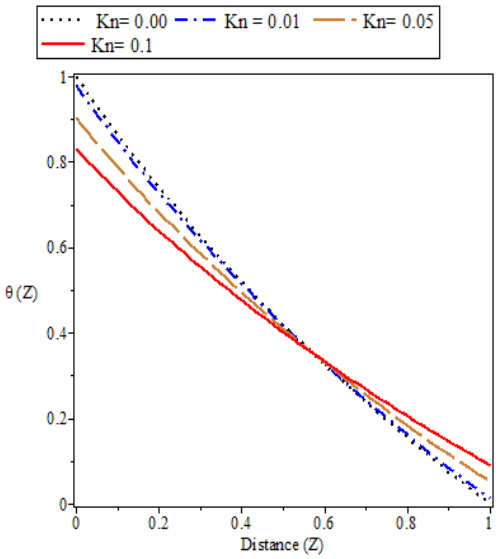

Fig. 13. Effect of Knudsen number on velocity field

Fig. 14. Effect of Knudsen number on temperature field

The effect of the Knudsen number on temperature and velocity distribution is shown in Figs. 13 and 14 accordingly. From Fig.13 increase in Kn correspond to a significant rise in both the fluid velocity and the slip velocity at the surfaces. While the effect Kn depreciates the temperature gradients at the outer surface of the inner cylinder and produces a significant increase in the fluid velocity near the inner surface of the outer cylinder. Meanwhile, a rise in temperature jump and reduction in the rate of heat transfer at the inner surface of the outer cylinder emanate when Kn increases, as a result of a reduction in buoyancy effect (see Fig. 14).

Figures 15 and 16, present the behavior of H_0 on velocity and temperature distributions for both heat absorption $(H_0 < 0)$ and generation $(H_0 > 0)$. For both cases, a higher magnitude of H_0 enhances the fluid velocity and temperature distributions respectively. Figures 17 and 18 account for the variation in magnitude of the Chemical reaction parameter (λ) which decelerates both the fluid velocity and concentration respectively.

Table 2. presents the volumetric flow analysis of heat and mass transfer in chemically reacting MHD flow through an inclined micro-annular channel, for which the effects of various parameters Kn, M, B, α and γ were shown. Interestingly, the volumetric flow rate (Q) is a decreasing function of M, B, α, and γ, except for Kn that produces an increase in Q as the magnitude rise. While the results of the Cf, Nu, and Sh were displayed in Tables 3-5, for various flow parameters at both surfaces. Skin friction in Table 3 reduces with a

higher magnitude of M , B , Kn , and α at the surface τ_0^* and increases accordingly at the surface τ_1^* . In Table 4, Kn and P increases the heat transfer coefficient (Nu) both at the Nu_0 and Nu_1 , while, a rise in H_0 increase Nu at Nu_0 and decrease at Nu_1 . Table 5, shows that Sc and λ decreases Sherwood number (Sh) at Sh_0 and increase at Sh_1 , while an increase is observed at both surfaces for an increase in Rc .

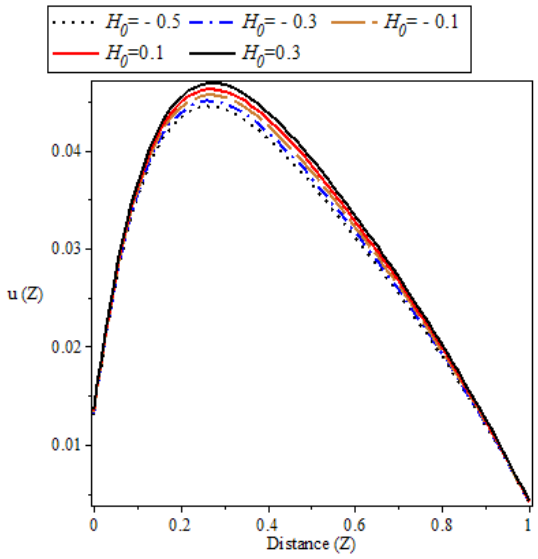

Fig. 15. Variation of Heat generation on the velocity profile

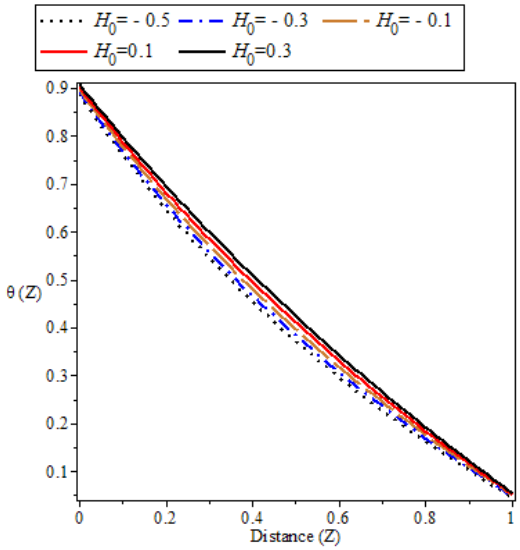

Fig. 16. Variation of Heat generation temperature profile.

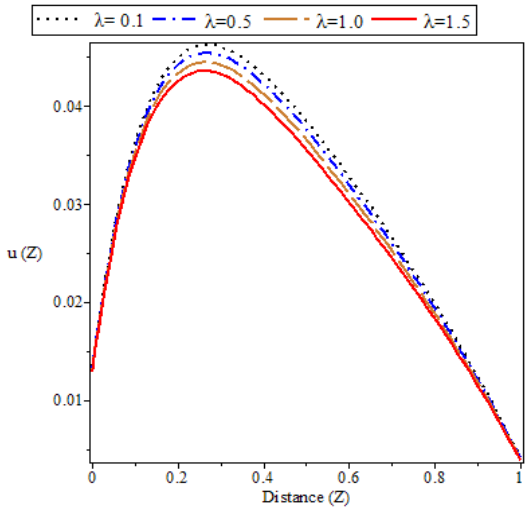

Fig. 17. Effect of chemical reaction on velocity profile

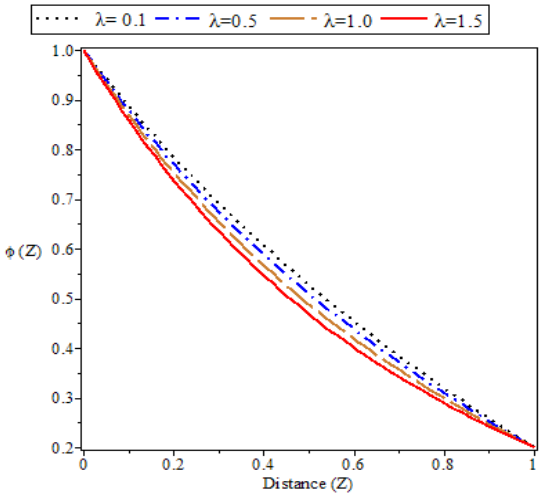

Fig. 18. Effect of chemical reaction on the concentration profile

Table 2 Volumetric flow rate (Q) analysis for different values of M , B , λ α and γ

Kn	M	Q	B	Q	α	Q	λ	Q	γ	Q
0.0	1.0	0.086197	0.5	0.072081	0	0.144163	0.2	0.071660	0.2	0.072082
	1.5	0.079845	1.0	0.039962	$\pi/6$	0.124848	0.5	0.070433	0.5	0.072082
	2.0	0.072081	1.5	-0.072622	$\pi/3$	0.072081	0.7	0.069642	0.7	0.072082
0.05	1.0	0.089457	0.5	0.074897	0	0.149794	0.2	0.074467	0.2	0.074897
	1.5	0.082890	1.0	0.047522	$\pi/6$	0.129725	0.5	0.073213	0.5	0.084827
	2.0	0.074896	1.5	-0.065704	$\pi/3$	0.074897	0.7	0.07240	0.7	0.851444
0.1	1.0	0.111812	0.5	0.093237	0	0.186473	0.2	0.092749	0.2	0.093237
	1.5	0.103314	1.0	0.085732	$\pi/6$	0.161491	0.5	0.091329	0.5	0.094461
	2.0	0.093237	1.5	0.054105	$\pi/3$	0.093237	0.7	0.090414	0.7	0.952127

Table 3 Skin friction coefficient (C_f) for different values of Kn, M , B and α

Kn	M	τ_0^*	τ_1^*	B	τ_0^*	τ_1^*	α	τ_0^*	τ_1^*
0.00	1.0	0.28084	-0.10992	0.5	0.25558	-0.09408	0	0.51116	-0.18817
	1.5	0.26953	-0.10276	1.0	0.19054	-0.05792	$\pi/6$	0.44268	-0.16296
	2.0	0.25558	-0.09408	1.5	0.11674	0.06096	$\pi/3$	0.25558	-0.09408
0.05	1.0	0.26786	-0.10817	0.5	0.24256	-0.09240	0	0.39923	-0.17040
	1.5	0.256515	-0.10102	1.0	0.18133	-0.06206	$\pi/6$	0.34574	-0.14757
	2.0	0.242561	-0.024075	1.5	0.11456	0.03462	$\pi/3$	0.19961	-0.08520
0.1	1.0	0.18368	-0.09156	0.5	0.16037	-0.07653	0	0.32075	-0.15307
	1.5	0.1731137	-0.08416	1.0	0.119641	-0.06615	$\pi/6$	0.277779	-0.132568
	2.0	0.1603758	-0.076538	1.5	0.083395	-0.04448	$\pi/3$	0.160376	-0.076538

Table 4 Heat transfer coefficient for different values of Kn, P , H_0 and ξ

Kn	P	Nu_0	Nu_1	H_0	Nu_0	Nu_1	ξ	Nu_0	Nu_1
0.01	0.00	-1.373464	-0.746407	0.1	-1.359644	-0.709506	0.2	-1.034059	-1.021943
	5.0	-1.237875	-0.678066	0.2	-1.325922	-0.722438	0.5	-1.325922	-0.722438
	10.0	-1.126046	-0.621749	0.3	-1.291667	-0.735706	0.8	-1.018001	-0.899204
0.05	0.00	-1.373464	-0.746407	0.1	-1.194784	-0.626639	0.2	-0.907769	-0.903274
	5.0	-0.883611	-0.499899	0.2	-1.163974	-0.640844	0.5	-1.163974	-0.640844
	10.0	-0.645786	-0.380981	0.3	-1.132471	-0.655514	0.8	-0.898705	-0.803966
0.1	0.00	-1.373464	-0.746407	0.1	-1.036975	-0.547343	0.2	-0.786710	-0.789572
	5.0	-0.645786	-0.380981	0.2	-1.008606	-0.562673	0.5	-1.008606	-0.562673
	10.0	-0.411712	-0.265618	0.3	-0.979355	-0.578639	0.8	-0.782429	-0.711301

Table 5 Sherwood number (Sh) for different values of ξ , Sc , λ and Rc

ξ	Sc	Sh_0	Sh_1	λ	Sh_0	Sh_1	Rc	Sh_0	Sh_1
0.2	0.2	-0.885627	-0.844625	0.1	-0.894728	-0.842369	1.0	-0.020126	0.015968
	0.5	-0.89109	-0.843271	0.5	-0.945228	-0.829895	2.0	1.073127	1.088891
	0.8	-0.896545	-0.841919	1.0	-1.007280	-0.814662	2.5	1.619754	1.625352
0.5	0.2	-1.161570	-0.573541	0.1	-1.180833	-0.564199	1.0	-0.040468	0.031933
	0.5	-1.173145	-0.567925	0.5	-1.286158	-0.513550	2.0	1.384988	0.777099
	0.8	-1.184669	-0.562342	1.0	-1.412108	-0.453952	2.5	2.097716	1.149683
0.8	0.2	-0.903699	-0.712710	0.2	-0.922145	-0.701995	1.0	-0.036241	0.033642
	0.5	-0.914782	-0.070626	0.5	-1.023077	-0.643922	2.0	1.071138	0.953187
	0.8	-0.925818	-0.699864	1.0	-1.143951	-0.575649	2.5	1.624828	1.412959

5 Conclusion

In this study, the combined effect of second-order slip and jump in chemically reacting MHD flow through an inclined micro-annular channel is considered, and AGM has been employed to approximate the dimensionless governing fully developed model semi-analytically. The results are presented in tables and graphs. Below are the main findings of the study;

i. The velocity profile depreciates with an increase in the second-order slip, inclination angle, fluid wall interaction, and chemical reaction parameters while the reverse is the case with a rise in viscosity, Radii ratio, Buoyancy ratio, wall concentration ratio, Knudsen number, and heat source/sink parameters.

ii. The temperature is enhanced with a hike in the heat source/sink parameter and diminished for greater values of fluid wall interaction and Knudsen number accordingly.

iii. AGM results preserve enough accuracy and efficiency compared to the existing literature.

iv. Increases in the chemical reaction parameter slow down the concentration profile.

v. Flow rate is elevated with increasing values of Knudsen number and depreciated with higher values of the magnetic field, viscosity, inclination angle, and second-order slip parameters.

vi. At τ^*_1, the skin friction increases with an increase in M, B, Kn and α, while a decrease is observed at τ^*_0. While Kn and P increases Nusset number at Nu_0. An increase in Sc and λ increases Sherwood's number Sh_0 while the reverse is the case at Sh_1.

Abbreviations

MHD – magnetohydrodynamics
AGM - Akbari-Ganji's method
ODEs – Ordinary differential equations
PDEs – Partial differential equations

Nomenclature

α	-Inclination angle	T_o	-Temperature at the inlet
B	-Variable viscosity parameter	β_t , β_v	-Dimensionless parameter
B_0	-Magnetic flux density	β_n	-Thermal expansion coefficient
Br	-Boyancy ratio	β_m	-Concentration expansion coefficient
c_p	-Specific heat at constant pressure	γ	-Second-order slip parameter
D_B	-Mass diffusivity	γ_r	-Ratio of specific heat
g	-Acceleration due gravity	η	-Dimensionless gap between the cylinders
H_0	-Generation/absorption	θ	-Dimensionless temperature
Kn	-Knudsen number	ι^*	-Skin friction coefficient
M	-Magnetic field parameter	κ	-Thermal conductivity
N	-Degree of polynomial	λ	-Chemical reaction parameter
Nu	-Heat transfer coefficient	λ_d	-Molecular mean free path
P	-Wall fluid interaction	ρ_0	- fluid mixture density
Pr	-Prandtl number	ν_0	-Kinematic viscosity
Q	-Flow rate	ξ	-Radii ratio parameter
ϕ_o	-Concentration at the inlet	ρ	-Fluid density
r_1, r_2	-Inner and outer cylinders radius	σ_m	-Thermal accommodation
Rc	-Wall concentration ratio	σ_t	-Tangential momentum accommodation
Sc	-Schmidt number	ϕ_1	-Outer-inner surface concentration
Sh	-Sherwood number	ϕ	-Dimensionless concentration
T	-Fluid temperature	ϕ_2	-Inner-outer surface concentration
T_2	-Inner-outer surface temperature	$\bar{\phi}$	-Fluid concentration
T_1	-Outer-inner surface temperature	u	-Dimensionless axial velocity
$\bar{u}$	-Dimensional axial velocity	ω	-Dimensional radial coordinates
Z	-Dimensionless radial coordinate		

Acknowledgment

Not applicable

Funding

No funding was received for this research.

Reference

[1] S. Adesanya, Free convective flow of heat generating fluid through a porous vertical channel with velocity slip and temperature jump. Ain Shams Eng. J. 6(3) 2015, 1045–1052.

[2] A. Ahmadi, G. M. Akbari, Nonlinear Dynamic in Engineering by Akbari-Ganji's Method. Bloomington, Indiana: Xlibris; 2015, Reprint edition.

[3] M. Akbari, D. Ganji, M. Nimafar, A. Ahmadi, Significant progress in solution of nonlinear equations at displacement of structure and heat transfer extended surface by new AGM approach. Frontiers of Mech. Eng. 9(4) 2014, 390–401.

[4] M. T. Akolade, A. S. Idowu, A. T. Adeosun, Multislip and Soret–Dufour influence on nonlinear convection flow of MHD dissipative Casson fluid over a slendering stretching sheet with generalized heat flux phenomenon. Heat Transfer. 2021;1–21. https://doi.org/10.1002/htj.22057

[5] M. T. Akolade, A. T. Adeosun, J. O. Olabode, Influence of Thermophysical Features on MHD Squeezed Flow of Dissipative Casson fluid with Chemical and Radiative Effects, J. Appl Comp. Mech, 2020, pp. -. doi: 10.22055/jacm.2020.34909.2508.

[6] T. Ameel, X. Wang, R. Barron, R. Warrington, Laminar forced convection in a circular tube with constant heat flux and slip flow. J. of Microscale Ther. Eng. 1(4) 1997, 303–320.

[7] M. Atashafrooz, T. Asadi, The Effects of Buoyancy Force on the Irreversibility of Three-Dimensional Step Flow in an Inclined Duct. J. Serbian Soci. Comp Mech., 13(1) 2019, 1-16, 10.24874/jsscm.2019.13.01.01

[8] A. Avramenko, N. Dmitrenko, I. Shevchuk, Heat transfer and hydromagnetics of slip confusor flow under second-order boundary condition. J. Ther. Analy. Colorim. 2020.

[9] S. Chakraverty, N. Mahato, P. Karunakar, T. Rao, Advanced Numerical and Semi-Analytical Methods for Differential Equations, First Edition. USA, Canada. New Jersey, John Wiley and Sons, Inc. 2019.

[10] S. Debnath, S. Paul, A. Roy, Transport of reactive species in oscillatory annular flow. J. Appl. Flu. Mech. 11(2) 2018, 405–417.

[11] K. Dharmalingam, M. Veeramuni, Akbari-Ganji's method (AGM) for solving non-linear reaction diffusion equation in the electroactive polymer film. J. Electroanalytical Chem. 844, 2019, 1–5.

[12] J. Gbadeyan, E. Titiloye, A. Adeosun, Effect of variable thermal conductivity and viscosity on casson nanofluid flow with convective heating and velocity slip. Heliyon 6(1) 2020, e03076.

[13] S. Ghadikolaei, K. H. Hosseinzadeh, D. Ganji, Analysis of unsteady mhd eyring-powell squeezing flow in stretching channel with considering thermal radiation and joule heating effect using AGM. Case Stud. in Therm. Eng. 10 2017, 579–594.

[14] C. Huel, Second - order slip flow and heat transfer in a long isoflux microchannel. W. Acad. of Sci., Eng. and Tech. Int. J. of Mech and Mechat. Eng. 8(8) 2014, 1464–1467.

[15] C. Hui, L. Chien-Hung, Second-order slip flow and heat transfer in a long isothermal microchannel. W. Acad of Sci, Eng. and Tech., Int. J. of Mech., Aeros., Ind., Mech. and Manuf. Eng. 8 2015, 1348–1351.

[16] G. Ibanez, A. Lopez, I. Lopez, J. Pantoja, J. Moreira, O. Lastres, Optimization of MHD nanofluid flow in a vertical microchannel with a porous medium, nonlinear radiation heat flux, slip flow and convective radiative boundary conditions. J. Therm. Analy. Colorim., 135 2019, 3401–3420.

[17] A. S. Idowu, U. Sani, Thermal radiation and chemical reaction effects on unsteady magnetohydrodynamic third grade fluid flow between stationary and oscillating plates Int. J. of Applied Mechanics and Engineering, 2019, 24(2) 269-293.

[18] A. S. Idowu, M. T. Akolade, T. L. Oyekunle, J. U. Abubakar, Nonlinear convection flow of dissipative Casson nanofluid through an inclined annular microchannel with a porous medium. Heat Transfer. 2020, 1–19.

[19] A. S. Idowu, M. T. Akolade, J. U. Abubakar, B. O. Falodun, MHD free convective heat and mass transfer flow of dissipative Casson fluid with variable viscosity and thermal conductivity effects, J Taibah Univ. Sci., 14(1) 2020, 851-862.
[20] B. Jha, B. Aina, S. Isa. Fully developed MHD natural convection flow in a vertical annular microchannel: An exact solution. J. King saud Uni. Sci. 27(3) 2015, 253–259.
[21] B. Jha, B. Aina, Z. Rilwanu, Steady fully developed natural convection flow in a vertical annular microchannel having temperature dependent viscosity: An exact solution. Alex. Eng. J. 55(2) 2016, 951–958.
[22] B. Jha, S. Joseph, S., Ajibade, A., Role of thermal diffusion on double-diffusion natural convection in a vertical annular porous medium. Ain Shams Eng. J. 6(2) 2015, 629–637.
[23] A. Khan, A. Sohai, S. Rashid, M. Rashidi, N. Khan, Effects of slip condition, variable viscosity and inclined magnetic field on the peristaltic motion of a non-Newtonian fluid in an inclined asymmetric channel. J. Appl. Flu. Mech. 9(3) 2016, 1381–1393.
[24] Y. Liu, B. Guo, Effects of second-order slip on the flow of a fractional maxwell MHD fluid. J. Asso. Arab Univ. Basic-Appl. Sci. 24 2017, 232–241.
[25] O. D. Makinde, E. Osalusi, Mhd steady flow in a channel with slip at the permeable boundaries. Rom. J. Phy. 51(3) 2006, 319–328.
[26] H. Mirgolbabaee, S. T. Ledari, D. Ganji. An assessment of a semi analytical ag method for solving nonlinear oscillators. New Trends in Math. Sci. 4(1) 2016, 283–299.
[27] H. Mirgolbabaee, S. T. Ledari, D. Ganji. Semi-analytical investigation on micropolar fluid flow and heat transfer in a permeable channel using agm. J. Asso Arab Univ. Basic Appl. Sci. 24 2017, 213–222.
[28] H. Mirgolbabaee, S. T. Ledari, D. Ganji. E. Valujai. Analyzing the nonlinear heat transfer equation by agm. New Trends in Math. Sci. 5(1) 2017, 51–58.
[29] A. M. Okedaye, S. O. Salawu. Effect of Nonlinear Radiative Heat and Mass Transfer On Mhd Flow Over A Stretching Surface With Variable Conductivity And Viscosity, J. Serbian Soci. Comp Mech., 13(2) 2019, 86-103.
[30] M. Oni, B. Jha. Heat generation absorption effects on material convection flow in a vertical annulus with time-periodic boundary conditions. J. Air-Space. Tech. 3 2019, 183–196.
[31] T. L. Oyekunle, S. A. Agunbiade. Combined Effect of Thermal Radiation And Viscous Dissipation on Unsteady Free Convective Magneto-Hydrodynamic Flow Through An Irregular Channel J. Serbian Soci. Comp Mech., 14(1) 2020,37-51.
[32] N. Rajasekhar, P. Prasad, D. P. Rao. Effect of chemical reaction and radiation absorption on unsteady convective heat and mass transfer flow of a viscous electrically conducting fluid in a vertical wavy channel with traveling thermal waves and hall effects. Int. J. Eng. Res. Appl. 3(1) 2013, 1733–1747.
[33] P. Reddy, P. Sreedevi, A. Chamkha. Mhd boundary layer flow, heat and mass transfer analysis over a rotating disk through porous medium saturated by cu-water and ag-water nanofluid with chemical reaction. Pow. Tech. 307 2017, 46–55.
[34] M. Saghafian, I. Saberian, R. Rajabi, E. Shirani. A numerical study on slip flow heat transfer in micro-poiseuille flow using perturbation method. J. Appl. flow Mech. 8(1) 2015, 123–132.
[35] M. Sheikholeslami, D. Ganji. Applications of Semi-Analytical Methods for Nanofluid Flow and Heat Transfer. Oxford: Elsevier Inc. 2018.
[36] G. Tunc, Y. Bayazitoglu. Heat transfer in microtubules with viscous dissipation. Int. J. Heat Mass trans. 44, 2001, 2395–2403.
[37] H. Xu, C. Zhao, Z. Xu. Analytical conditions of slip flow and heat transfer through microfoams in mini/microchannels with asymetric wall heat flux. Appl. ther. Eng. 93 2016, 15–25.
[38] T. Yusuf. Exact solution of an mhd natural convection flow in vertical concentric annulus with heat absorption. Int. J. Fluid mech. Ther. Sci. 3(5) 2017, 52–61.
[39] T. Yusuf, B. Jha. A semi-analytical solution for time - dependent natural convection flow with heat generated absorption in an annilus partially filled with porous material. Multidisc. Mod. Mat. Stru. 14(15) 2018, 1042–1063.
[40] J. Zhu, D. Yang, L. Zheng, X. Zhang, Second-order slip effect on heat transfer of nanofluid with Reynolds model of viscosity in a coaxial cylinder. Int. J. Nonl. Sci. Num. Sim. 16(6) 2015, 285–292.